

Hybrid HHL with Dynamic Quantum Circuits on Real Hardware

Romina Yalovetzky, Pierre Minssen, Dylan Herman, Marco Pistoia

Global Technology Applied Research, JPMorgan Chase Bank, N.A, 237 Park Avenue, New York, NY 10017

Abstract—In recent years, quantum algorithms have been developed for accelerating basic linear algebraic operations applied to vectors encoded in quantum states. Unfortunately, the majority of the components of quantum linear system solvers are far out of the reach of noisy intermediate-scale quantum devices. This precludes the ability to produce small-scale experiments for benchmarking all the components on real quantum hardware. This work advances a hybrid variant of the Harrow-Hassidim-Lloyd (HHL) algorithm that is more suitable for small quantum devices. First, we reduce the circuit complexity of the eigenvalue estimation component by leveraging newly available quantum-hardware features for implementing dynamic quantum circuits, such as mid-circuit measurements, qubit reset and reuse, and quantum conditional logic. Second, we introduce a novel method for scaling the linear-system matrix such that the eigenvalue estimation is more accurate. We empirically demonstrate the effectiveness of these Hybrid HHL enhancements by applying this algorithm to small portfolio optimization problems, executed end-to-end on the Quantinuum System Model H1-2 trapped-ion quantum computer. Lastly, we present a comparative analysis of the various approaches for eigenvalue inversion to better understand when it is beneficial to utilize Hybrid HHL.

Keywords. Portfolio Optimization, Quantum Linear Systems, HHL, Semi-Classical Quantum Fourier Transform, Mid-Circuit Measurement and Reuse, Quantum Conditional Logic.

I. INTRODUCTION

The HHL algorithm was introduced by Harrow, Hassidim and Lloyd [1] to solve the Quantum Linear Systems Problem (QLSP). A linear system is of the form $A\vec{x} = \vec{b}$, where $A \in \mathbb{C}^{N \times N}$ and $\vec{x}, \vec{b} \in \mathbb{C}^N$, thereby returning the quantum state $|x\rangle$ corresponding, up to a normalization factor, to the solution of the linear system.

HHL is known to be cumbersome to deploy [2], especially on Noisy Intermediate-Scale Quantum (NISQ) hardware [3]. Recently, hybrid versions of QLSP solvers, such as variational approaches [4, 5] and Hybrid HHL [6, 7] have been developed to enable near-term experimentation with quantum linear algebra techniques. The Hybrid HHL, originally developed by Lee *et al.*, is focused on reducing the complexity of the eigenvalue inversion step. Given enough qubits, this can be implemented with polynomial-sized circuits utilizing *quantum arithmetic* to approximate arcsine [8]. However, due to hidden constant factors behind the asymptotic notation, most near-term approaches fall back on an implementation based on optimized-versions of the *uniformly controlled rotation* (UCR) gate, whose n -qubit circuit depth, in terms of basis gates, is $\Omega(2^n)$ [9].

At the cost of no longer providing any exponential speedup, Hybrid HHL avoids utilizing a UCR gate by first estimating the eigenvalues of the linear system matrix in a preliminary step. Since the eigenvalues are now known, the inversion circuit can be constructed to only consist of controlled rotations targeting the observed eigenvalues. Thus, in a subsequent step, a coherent-version of HHL is executed with the reduced inversion circuit. Since the cost of a n -qubit-controlled rotation grows linearly in n [10], the complexity of the eigenvalue inversion circuit for m eigenvalues is $O(mn)$ as opposed to exponential in n , as it is in the case of UCR.

In this work, we demonstrate that this preliminary eigenvalue estimation step can be further optimized with newly-available hardware features, specifically dynamic quantum circuits (DQCs) [11]. The ability to execute DQCs enables the insertion of mid-circuit measurements, resets, and logic conditioned on intermediate measurement results, i.e., quantum conditional logic (QCL). The semi-classical inverse quantum Fourier transform (QFT) [12] is a DQC that can be used to reduce the required number of ancillary qubits for quantum phase estimation (QPE) [13, 14] to one and replaces all two-qubit gates in the inverse QFT with classically-controlled single-qubit gates. For brevity, we call this variant of QPE the QCL-QPE. This can result in a more NISQ-friendly circuit as qubits are a scarce resource on near-term devices and faulty two-qubit gates are currently the dominant source of error.

In addition to the integration of DQCs, we further enhance the eigenvalue estimation step by presenting an algorithmic technique for estimating the matrix scaling factor that is required to achieve accurate eigenvalue estimates with QPE.

The combination of the methods we introduce produces a more hardware-optimized version of Hybrid HHL. We demonstrate this by applying our algorithm to the mean-variance portfolio optimization and provide detailed resource analysis of the various components.

A. Novel Contributions of This Work

This paper makes the following novel contributions:

- 1) The integration of QCL-QPE, which makes use of DQCs, into the Hybrid HHL framework introduced by Lee *et al.* This procedure only requires one ancillary qubit to estimate eigenvalues to arbitrary precision.
- 2) An efficient and verifiable procedure for determining a factor to scale the system matrix by, which allows for resolving the eigenvalues with significantly higher accuracy.

- 3) To the best of our knowledge, we demonstrate the largest-to-date execution [6, 7, 15] of HHL with a two-qubit gate depth up to 254 on real quantum hardware—the trapped-ion Quantinuum System Model H1-2. For this experiment, HHL was used to solve a portfolio optimization problems with S&P 500 assets.
- 4) A comparative analysis of the required two-qubit gate and ancillary qubit count of different implementations of the eigenvalue inversion component of HHL.

B. Paper Organization

The remainder of this paper is organized as follows. Section II describes the eigenvalue inversion component of HHL and the different approaches that have been proposed in the literature. Section III introduces the novel techniques for enhancing Hybrid HHL. In particular, Section III-A introduces QCL-QPE, and shows benchmarks on quantum hardware, the trapped-ion Quantinuum System Model H1-2. This section also explains how the QCL-QPE is integrated to the Hybrid HHL to estimate the relevant eigenvalues. Section III-B introduces the algorithmic contributions, focusing on its novelties. It also contains results obtained from experiments on hardware showing how these algorithms allow for estimating the eigenvalues accurately. Section IV describes a known formulation of portfolio optimization as a QLSP, which makes it compatible with HHL and it presents a detailed comparative analysis of the hardware demonstrations of the end-to-end Hybrid HHL with dynamic quantum circuits to solve this particular problem. Section V discusses different approaches for the eigenvalue inversion in terms of hardware features. Finally, Section VI summarizes the results of this work, and concludes the article.

II. EIGENVALUE INVERSION COMPONENT OF HHL

Given a Hermitian matrix $A \in \mathbb{C}^{N \times N}$, the n -bit estimation of an eigenvalue λ_i of A , with $i \in \{0, 1, \dots, N-1\}$, can be represented by a binary string of length n , of the form $\tilde{\lambda}_i := \lambda_i^{(n-1)} \dots \lambda_i^{(1)} \lambda_i^{(0)}$. Such a binary string can be encoded in a computational basis state as follows: $|\tilde{\lambda}_i\rangle_T := |\lambda_i^{(n-1)} \dots \lambda_i^{(1)} \lambda_i^{(0)}\rangle_T$, where T is an n -qubit register.

The eigenvalue inversion component of HHL involves controlled rotations conditioned on the n -bit estimations of the eigenvalues, i.e., multiset $\{\tilde{\lambda}_i\}_{i=0}^{N-1}$. This algorithmic component can thus be represented by the following map:

$$\sum_{i=0}^{N-1} |0\rangle \otimes \beta_i |u_i\rangle_S \otimes |\tilde{\lambda}_i\rangle_T \rightarrow \sum_{i=0}^{N-1} \left(\sqrt{1 - \frac{C^2}{\tilde{\lambda}_i^2}} |0\rangle + \frac{C}{\tilde{\lambda}_i} |1\rangle \right) \otimes \beta_i |u_i\rangle_S \otimes |\tilde{\lambda}_i\rangle_T \quad (1)$$

where C is a normalization constant chosen to be in $O(1/\kappa)$, and κ is the condition number of A [1].

This transformation is accomplished by applying R_y rotation gates to the ancillary qubit $|0\rangle$ controlled by the T register containing the eigenvalue estimates. A rotation will have to

be applied for each of the distinct elements of $\{\tilde{\lambda}_i\}_{i=0}^{N-1}$. The angle for the i^{th} rotation is $\theta_i = 2 \arcsin(C/\tilde{\lambda}_i)$. This computation requires either some prior information about the eigenvalues or a coherent computation of the arcsine function using quantum arithmetic [16]. However, quantum arithmetic has not yet been shown to be feasible on NISQ devices. The asymptotically efficient implementation of arcsine made by Häner *et al.* [16] requires over one-thousand CNOT gates even for a small register T of size two. As, we will not be leveraging this component, in favor of near-term friendly but non-asymptotically efficient implementation, we are losing the expected speed-up from HHL.

Another approach would be to perform an exhaustive search of the basis states of the eigenvalue estimation register. This can be accomplished by a uniformly controlled rotation gate [9]. A uniformly controlled rotation on n qubits decomposes into $2^n - 1$ n -qubit controlled rotations, as shown in Figure 1.

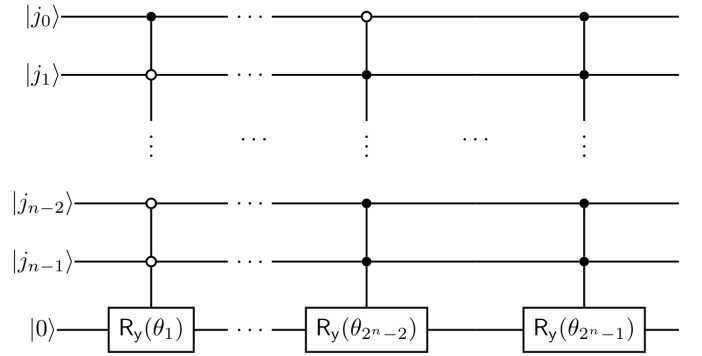


Fig. 1. Decomposition of a uniformly controlled rotation gate into $2^n - 1$ n -qubit controlled rotations. QPE loads the k^{th} bit of the n -bit approximation of each eigenvalue onto qubit j_k , for $k = 0, \dots, n-2, n-1$. For eigenvalue inversion, $\theta_i = 2 \arcsin(2^n C/i)$, for $i = 1, \dots, 2^n - 2, 2^n - 1$.

This would effectively control on all of the eigenvalue approximations that can be made with n bits, which exclude the zero state because A is assumed to be invertible. However, this approach can quickly become infeasible since, the circuit depth is exponential in the number of bit n to approximate the eigenvalues. The *Gray code* [17] can be used to reduce the number of basis gates required for this exponentially long sequence of n -qubit controlled rotations. However, it comes with the cost of computationally intensive classical operations, and the depth of the circuit is still $\Theta(2^n)$. Nonetheless, for small n , the Gray code can be the most efficient eigenvalue inverter. We refer the reader to Section VI for a comparative analysis of the resource requirements of these different approaches in terms of two-qubit gate and ancillary qubit counts.

Lee *et al.* have proposed a classical/quantum hybrid solution for HHL, the Hybrid HHL, which tweaks the multi-control rotation by combining rotations given the binary decomposition of the eigenvalues. Before running HHL, they apply QPE to the propagator U of A with input state $|b\rangle$. The output probability distribution is used to obtain estimates of the eigenvalues before performing the eigenvalue inversion. These estimates are employed to compute and combine the

angles and controls for the required rotations to perform the eigenvalue inversion. This two step method removes any expected speed-up due to the eigenvalue sampling.

Our work focuses on improving the Hybrid HHL and bring HHL closer to being realizable on current quantum hardware by leveraging newly available hardware features and developing algorithmic techniques. This is explained in detail in the following sections.

III. TECHNIQUES FOR ENHANCING HYBRID HHL

In the following subsections we will present and benchmark our techniques for improving the performance of Hybrid HHL on near-term quantum hardware. Figure 2 illustrates the end-to-end flow of the proposed implementation. Our aim is to execute and validate our approach on real quantum hardware supporting mid-circuit measurement, qubit reset and reuse, and QCL.

A. QCL-QPE for Eigenvalue estimation

To estimate the eigenvalues, one could utilize the aforementioned QPE approach of Lee *et al.* However, QPE is still difficult to implement on NISQ hardware [18] because the number of ancillary qubits grows with the desired bit precision. Additionally, an n -qubit QFT involves at least one controlled rotation between any two qubits, and $\binom{n}{2}$ in total. Therefore, a quantum device with all-to-all connectivity is preferred to limit the use of SWAP gates.

A QPE variant [13, 14] has been identified that better lends itself to NISQ hardware and utilizes the semi-classical inverse QFT [12]. This is a nonunitary version of the inverse QFT that estimates each bit of the eigenvalue sequentially. A diagram of this variant is displayed in Figure 3a, which shows how to efficiently estimate the eigenvalues of the unitary operator U to three bits of precision by leveraging techniques for DQCs: mid-circuit measurements, ground-state resets, QCL, and qubit reuse. This QPE variant, which we call QCL-QPE, has been previously demonstrated on quantum hardware [11]. However, to the best of our knowledge, our work is the first one incorporating it into a quantum algorithm executed end-to-end on commercially available hardware for solving a practical problem.

QCL-QPE is mathematically equivalent to performing the original inverse QFT and measuring the eigenvalue register. It is also similar to iterative QPE (iQPE) [19] to the extent that it only requires one ancillary qubit to achieve arbitrary bit precision of the eigenvalues. A limitation of iQPE, however, is that it requires the initial state to be an eigenvector of U in order to estimate its corresponding eigenvalue. Conversely, QCL-QPE can estimate eigenvalues without prior information of the eigenvectors.

This approach to phase estimation has two properties that make it more suitable for near-term devices than the standard version of QPE:

- 1) the procedure requires only one ancillary qubit for an arbitrary bit precision,

- 2) and it replaces two-qubit gates with one-qubit gates controlled by classical registers.

These differences can be observed by comparing Figures 3a and 3b.

Our work proposes to use QCL-QPE to estimate the matrix's eigenvalues and then, similar to the original Hybrid HHL, control the rotations on these estimates in the eigenvalue inversion component. However, in the inversion circuit, we will only introduce controlled rotations for eigenvalues that satisfy certain conditions. If

$$|x\rangle_S = |A^{-1}b\rangle_S = \sum_{i=0}^{N-1} \frac{\beta_i}{\lambda_i} |u_i\rangle_S$$

is the solution to the QLSP, then we define the set of the *relevant eigenvalues* of A as $\Lambda_b := \{\lambda_i : |\beta_i/\lambda_i| > \epsilon\}$, where $\epsilon \geq 0$ is a configurable threshold. Essentially, Λ_b contains the m distinct eigenvalues of A whose amplitudes in the solution, in absolute value, are sufficiently large.

Note that, apart from the eigenvalue estimation component, where the standard QPE is replaced by QCL-QPE, as shown in Section II, our version of Hybrid HHL still uses the standard QPE. This is because QCL-QPE repeatedly collapses the quantum state of the ancillary qubit through mid-circuit measurements. Therefore, this eigenvalue estimation procedure cannot be incorporated as part of a deeper circuit that relies on the quantum states encoded in this ancillary register.

Performance on Hardware: We benchmarked the performance of both the standard QPE and QCL-QPE for estimating the eigenvalues of the operator $U := e^{iA2\pi\gamma}$ of a 4×4 matrix A scaled by a parameter γ and applied to an initial state $|b\rangle$. A technique for selecting the scaling parameter will be presented Section III-B. The matrix and initial state used correspond to a constrained portfolio-optimization problem with two S&P 500 assets. The way portfolio optimization problem is cast as a QLSP is explained in Section IV-A.

All the experimental results that are presented in this article were obtained on the trapped-ion Quantinuum System Model H1-2 given its support for mid-circuit measurements, qubit resets and reuses, and QCL [20]. This quantum processor uses a quantum charge-couple device architecture with three parallel gate zones in a linear trap. The quantum states are stored in the hyperfine states of twenty $^{171}\text{Yb}^+$ atoms. All-to-all connectivity is implemented by rearranging of the physical location of qubits, which introduces a negligible amount of error. Typical single-qubit gate infidelity is 5×10^{-5} and typical two-qubit gate infidelity is 3×10^{-3} . Typical error rate of state preparation and measurement is 3×10^{-3} . Memory error per qubit at average depth-1 circuit ("idle error") is 4×10^{-4} . Additional details are available in [21].

In order to run the circuits on hardware, we transpiled and optimized the circuits from IBM's Qiskit [22] to H1-2's native gates using Quantinuum's pytket package [23].

Note that the implementation of the Hamiltonian simulation routine is not in the scope of this work. It would require addressing the challenges of performing it on NISQ devices [24]. In order to perform experiments on quantum hardware, instead

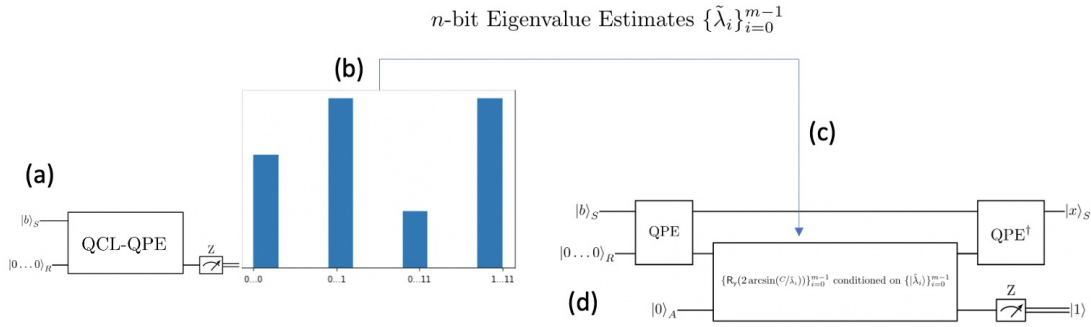
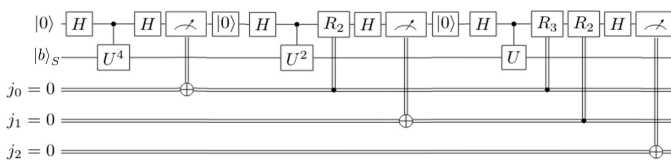
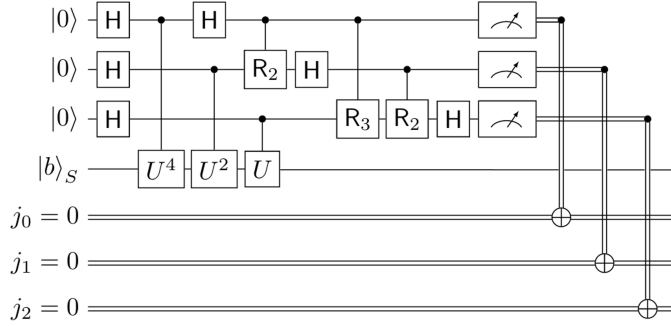


Fig. 2. End-to-End Flow of the Proposed HHL implementation: (a) QCL-QPE is used to construct a distribution over the estimates of the relevant eigenvalues with n -bit precision. The optimal scaling parameter, γ , for QPE is determined by running algorithms 1 and 2. (b) Classical post-processing is performed on the resulting histogram to obtain the estimates of the m relevant eigenvalues, i.e., Λ_b . (c) The n -bit estimates, $\{\tilde{\lambda}_i\}_{i=0}^{m-1}$, obtained in (b), are used to determine rotation angles $\{2 \arcsin(C/\tilde{\lambda}_i)\}_{i=0}^{m-1}$ for the eigenvalue inversion circuit. (d) The standard HHL procedure is executed, but it uses the circuit constructed in (c) for the eigenvalue inversion step.



(a) QCL-QPE circuit



(b) QPE circuit

Fig. 3. Circuits for estimating the eigenvalues of the unitary operator U to three bits using QCL-QPE (a) or QPE (b). S is the register that U is applied to, and j is a classical register. H refers to the Hadamard gate and R_k , for $k = 2, 3$, are the phase gates.

of using quantum algorithms for Hamiltonian simulation, we classically computed $U := e^{iA2\pi\gamma}$, where γ is the scaling parameter. Then, we pass it to the Qiskit transpiler, which decomposes it into basis gates.

As the error rates of two-qubit gates are an order of magnitude larger than those of one-qubit gates [20], and the numbers of both gate types are similar in the circuits used, we will only present the H1-2 two-qubit gate ZZMax counts for the circuits. The ZZMax is equivalent to $R_{ZZ}(\pi/2)$, and, up to one-qubit gates, it is realized via the Mølmer-Sørensen interaction [20].

In Table I, we compare the number of gates and qubits required for both QPE implementations for estimating the eigenvalues of A to different precisions: three, four and five. We can see that QCL-QPE employs fewer qubits and gates.

| | 3-bit | 4-bit | 5-bit |
|--------------|----------|-------|-------|
| Standard QPE | Gates 63 | 88 | 115 |
| | Qubits 5 | 6 | 7 |
| QCL-QPE | Gates 57 | 76 | 95 |
| | Qubits 3 | 3 | 3 |

TABLE I

COMPARISON OF THE NUMBER OF TWO-QUBIT ZZMAX GATES AND QUBITS IN BOTH QPE IMPLEMENTATIONS FOR ESTIMATING EIGENVALUES TO DIFFERENT PRECISIONS.

As the precision grows, the number of two-qubit gates increases for both implementations. However, the number of two-qubit gates saved using QCL-QPE, instead of the standard implementation, grows quadratically as $n(n-1)$, with n being the bit precision. Moreover, even though the precision in bits increases, the number of qubits in the QCL implementation does not change. This contrasts with the linear growth in the standard QPE.

In order to quantify the performance of both implementations, we compared the empirical distribution of measurement results from the circuit execution on the Quantinuum System Model H1-2 to the distribution obtained from the Qiskit Aer simulator. One way to compare two probability mass functions, p and q , is to use the fidelity metric [25]: $F(p, q) = (\sum_i \sqrt{p_i q_i})^2$, $F(p, q) \in [0, 1]$.

We compare the achieved fidelity in both implementations for the three precisions, in Table II. It can be seen that the computed fidelity metrics for the two implementations are similar for three-bit estimations. Here the number of saved two-qubit gates using QCL-QPE is small. In addition, reducing the number of qubits does not overcome potential errors due to mid-circuit measurements and resets.

When we increase the precision to four and five bits, the circuits in both implementations deepen, and therefore, we see a drop in fidelity. Nevertheless, as shown in Table I, QCL, mid-circuit measurement, and qubit reset and reuse, result in the QCL-QPE circuit being shallower than the standard implementation. As a consequence, the achieved fidelity with

| | 3-bit | 4-bit | 5-bit |
|--------------|-------|-------|-------|
| Standard QPE | 98.6 | 90.4 | 42.6 |
| QCL-QPE | 98.1 | 95.0 | 43.2 |

TABLE II

FIDELITY EXPRESSED IN % BETWEEN THE PROBABILITY DISTRIBUTIONS FROM THE QPE EXPERIMENTS RAN ON THE QUANTINUUM SYSTEM MODEL H1-2 AND IN THE QISKIT QASM SIMULATION, WITH 2000 SHOTS EACH.

QCL-QPE is still higher than the standard QPE. In both implementations, the decay of the fidelity for five-bit precision can be explained by the number of gates approaching the limit supported by current devices.

B. Optimizing the Scaling Parameter

In this section we present the novel algorithmic contributions of this work: the integration of a verifiable algorithm for selecting the optimal scaling parameter to scale the matrix A of the QLSP. This scaling allows for effectively estimating the eigenvalues in the output distribution obtained with the separate QPE component.

In the foundational HHL article [1], A is assumed to have positive eigenvalues in $[1/\kappa, 1]$, where κ is the condition number of A . The eigenvalues are restricted to this range to account for the periodicity of the imaginary exponential and ensured well-conditioning. In practice, it is necessary to scale A to have a spectrum in this range. However, even under this assumption, we could be wasting qubits to unnecessarily encode values between the largest eigenvalue, λ_{\max} , and 1. We pursue a more efficient approach, consisting of estimating λ_{\max} first, and then scaling A by $\gamma = \tilde{\lambda}_{\max}^{-1}$, so that the maximum eigenvalue of γA is 1.

A benefit of our approach is that it only considers $\lambda_{\max,b}$, the largest eigenvalue in Λ_b , instead of λ_{\max} . For now on, we will only take into account the eigenvalues in Λ_b and will not, for example, make a distinction between $\lambda_{\max,b}$ and λ_{\max} .

Algorithm 1 shows how to optimize the selection of γ . Given n -bits, the optimal value of γ returned by the algorithm helps to encode the eigenvalues using all available bits in the output distribution of QCL-QPE applied to $U := e^{iA2\pi\gamma}$. As a result, this makes it easier to distinguish the eigenvalues from each other and estimate the relevant eigenvalues, i.e., Λ_b , accurately. Without loss of generality, Algorithm 1 assumes all the eigenvalues to be positive. We will show shortly how to account for negative eigenvalues.

Algorithm 1 starts by guessing an overapproximation of λ_{\max} . We will discuss later how to make this operation rigorous. The next step consists of iteratively updating the value of γ until γ converges to the optimal value. During each iteration, Algorithm 1 runs QCL-QPE to compute the n -bit estimates of the eigenvalues of the unitary U using gamma computed during the previous iteration. Specifically, Algorithm 1 post-processes the output distribution to get a new n -bit estimation

Algorithm 1: Optimize the selection of γ using n -bit estimations of eigenvalues

```

Guess an overapproximation  $\alpha$  of  $\lambda_{\max}$ 
 $\gamma := 1/\alpha$  // Initialize scaling parameter
 $x := 0$ 
// At each step,  $\gamma * \lambda_{\max} \leq 1$ 
while  $x \neq 2^n - 1$  do
   $p := n$ -bit output distribution of QCL-QPE using
  unitary  $e^{iA2\pi\gamma}$  and input state  $|b\rangle$ 
   $x := \max\{j \in \{0, \dots, 2^n - 1\} \mid p_j > 0, p_j \in p\}$ 
  //  $x$  is an  $n$ -bit estimation of
  //  $2^n * \gamma * \lambda_{\max}$ 
  if  $x = 0$  then
    |  $\gamma := \gamma * 2^n$ 
  else
    |  $\gamma := \gamma * (2^n - 1)/x$ 
  end
end
Result:  $\gamma := \tilde{\lambda}_{\max}^{-1}$ , with  $\tilde{\lambda}_{\max}$   $n$ -bit estimation of  $\lambda_{\max}$ 

```

of $2^n \gamma \lambda_{\max}$ in order to update γ for the next iteration.¹

The number of iterations to find the optimal γ using Algorithm 1 is in $\Theta(1/n \log_2(\alpha/\lambda_{\max}))$. To ensure we do not overestimate γ in the process, we could take a conservative approach, which consists of overestimating x while computing it, thus lowering $(2^n - 1)/x$. In practice, we also want to underestimate γ in order to prevent amplitudes of basis states near 2^n from dispersing and mixing with basis states near 0 and causing overflowing.

Regarding the bit precision, to represent both the largest and smallest eigenvalues, in theory, we need $n \geq \log_2(\lambda_{\max}/\lambda_{\min}) = \log_2(\kappa)$. However, this requires prior knowledge of κ . In practice, we first run Algorithm 1 with an initial precision of n bits. Then, if λ_{\min} , estimated via QCL-QPE, turns out to be 0, this indicates that we need higher bit precision to prevent the 0 state from having significant probability. This is because A is assumed invertible and consequently, no eigenvalue can be 0. Thus, we increase n just enough to guarantee that the estimation of λ_{\min} is different from 0, at which point $n \geq \log_2(\kappa)$.

The correctness of Algorithm 1 relies on the fact that α is an overapproximation of λ_{\max} . One way to achieve this result is to use the Frobenius norm of A , defined as $\|A\|_F := \sqrt{\text{Tr}(A^\dagger A)}$. Indeed, since A is Hermitian, $\|A\|_F = \sqrt{\sum_{i=0}^{N-1} \lambda_i^2}$, and so the Frobenius norm of A is a valid overapproximation of λ_{\max} . However, the computation of the Frobenius norm has quadratic complexity in N . Therefore, it is desirable to find a faster approach for finding a value for α that overapproximates λ_{\max} . For this reason, we propose Algorithm 2, which, using one execution of QCL-QPE, tests the validity of any initial guess of α . This bypasses the need to compute $\|A\|_F$. If the initial

¹Any algorithm outputting an n -bit estimation of $2^n \gamma \lambda_{\max}$ could be used in place of QCL-QPE. Nevertheless, we chose to use QCL-QPE, since it is more compatible with NISQ devices, as explained in Section II.

guess of α does not satisfy $\alpha \geq \lambda_{\max}$, we can retry with a, potentially significantly, larger α . In fact, given the logarithmic complexity, in terms of number of iterations, of Algorithm 1, even with low bit precision, such as $n = 4$, overestimating λ_{\max} by a factor of a billion would only require eight iterations before returning the optimal γ . In practice, we expect to find γ significantly more efficiently by starting with a guess, α , than by computing $\|A\|_F$.

Algorithm 2: Verify if α is a n -bit overestimation of λ_{\max}

Assumption: at each step, there is at least one eigenvalue of γA not in $\bigcup_{j \in \mathbb{Z}} [j - 2^{-(n+1)}, j + 2^{-(n+1)}]$

```
// Initialize scaling parameter
 $\Gamma := 1/2^{n+1}\alpha$ 
 $p := n$ -bit output distribution of QCL-QPE using
unitary  $e^{iA2\pi\Gamma}$  and input state  $|b\rangle$ 
if  $p_0 \neq 1$  then
  | Return  $\alpha$  is not valid
  | // Otherwise all eigenvalues
  | // estimations would have been 0
else
  | Return  $\alpha$  is valid
end
```

Result: Return if α is an overestimation of λ_{\max}

The idea of Algorithm 2 is the following. If α is a valid guess, there will be no overflow in the output distribution of QCL-QPE applied to $e^{iA2\pi\gamma}$ with $\gamma = 1/\alpha$. Then, performing $n + 1$ right bit shifts should reduce all n -bit eigenvalue estimates to 0. To test this, Algorithm 2 executes QCL-QPE using $e^{iA2\pi\Gamma}$ with $\Gamma = 1/2^{n+1}\alpha$. On the contrary, if α is not a valid guess, the $n + 1$ right bit shifts would not be sufficient to reduce all estimations to 0. Note, γ and Γ have the same role in the definition of U and just help differentiate the two algorithms.

As mentioned before, Algorithm 1 assumes positive eigenvalues. To take into account negative eigenvalues, one can define the maximum eigenvalue using the absolute value, encode negative eigenvalues using two's complement and then replace 2^n by 2^{n-1} in the update of γ . Similarly, in Algorithm 2, replacing $1/2^{n+1}$ by $1/2^n$ in the definition of Γ suffices to support negative eigenvalues. Accounting for negative eigenvalues is crucial, since A , in the QLSP represented by (2), may be indefinite.

We note that Kerenidis and Prakash [26] have developed an algorithm to ϵ -approximate $\eta := \|A\|_2/\|A\|_F$, where $\|A\|_2 = |\lambda_{\max}|$ is the spectral norm of A . Thus, their algorithm can also be used to find $|\lambda_{\max}|$ given that $\|A\|_F$ has been previously computed, which is not required for Algorithm 1. As mentioned before, the optimal γ is $|\lambda_{\max,b}|^{-1}$ and not $|\lambda_{\max}|^{-1}$, when given $|b\rangle$ as an initial state. Since Algorithm 1 only computes $|\lambda_{\max,b}|^{-1}$, this makes it more suitable for the proposed HHL implementation based on the discussions in Section II.

In addition, their algorithm executes standard QPE, which is not exchangeable for QCL-QPE because of the coherence requirement. In contrast, Algorithm 1 runs QCL-QPE, which for the reasons explained above, is more suitable for NISQ computers.

Performance on Hardware: In this section we show results obtained on hardware that shows how Algorithm 2 and Algorithm 1 optimize the scaling parameter γ allowing for effectively estimating the relevant eigenvalues in the output distribution of QCL-QPE. We used the same matrix and initial state that were used for the previous benchmarks.

We started with an initial guess of 0.02 for λ_{\max} , corresponding to $\gamma = 50$. We verified with Algorithm 2 that $\alpha = 0.02$ was indeed an overestimation of λ_{\max} , as required by Algorithm 1. Following Algorithm 2, in the case of negative eigenvalues, we tested the validity of the initial guess $\gamma = 50$ with precision $n = 4$ by running QCL-QPE with $\Gamma = \gamma \cdot 2^{-4} = 50 \cdot 2^{-4}$. The output probability distribution, shown in Figure 4 (a), is concentrated around zero, thus $\gamma = 50$ is a valid guess. An example for an invalid input would be $\gamma = 3200$. The output distribution of QCL-QPE with $\Gamma = \gamma \cdot 2^{-4} = 200$ is plotted on Figure 4 (b). As this distribution is not concentrated around zero, $\gamma = 1600$ is not a valid guess.

Now that we confirmed $\gamma = 50$ is a valid guess, we can execute Algorithm 1. We ran QCL-QPE for estimating the eigenvalues of A with this value of γ , and we used $|b\rangle$ as the initial state. The output probability distribution is displayed in Figure 5 (a). The x -axis is binned into 16 values, which are all of the possible four-bit estimates in decimal. They are represented by the grey, vertical lines. In the experiment, we only observed significant probabilities (blue bars) for states within the range $[-0.005, 0.005]$.

Thus, in order to better distinguish the eigenvalues, we decreased the distance between bins by increasing the scaling factor γ . We did so by using our scale optimization algorithm, Algorithm 1, which increased γ to 100. As explained before, we overestimated λ_{\max} and hence underestimated γ to avoid overflow.

We can see in Figure 5 (b) that using $\gamma = 100$ makes the x -axis range smaller than in (a), while keeping the same number of bins. As a consequence, the bin intervals are smaller, and there is a better agreement between the theoretical eigenvalues, which are classically calculated, and the experimental probabilities. Moreover, we can see close concordance between the experimental and the simulation results (orange dots). The ability to better distinguish eigenvalues in (b) over (a) shows the importance of the scale optimization procedure. For clarification, the distribution of classically calculated, theoretical, values in the plots are distributed according to $\{|\beta_i|^2\}_{i=0}^{N-1}$, as mentioned at the beginning of Section IV.

Once we have obtained the probability distribution over the eigenvalue estimates with the optimal γ , we classically post-processed this distribution, displayed in Figure 5 (b), to select the estimates of the elements in Λ_b . In the general case, our

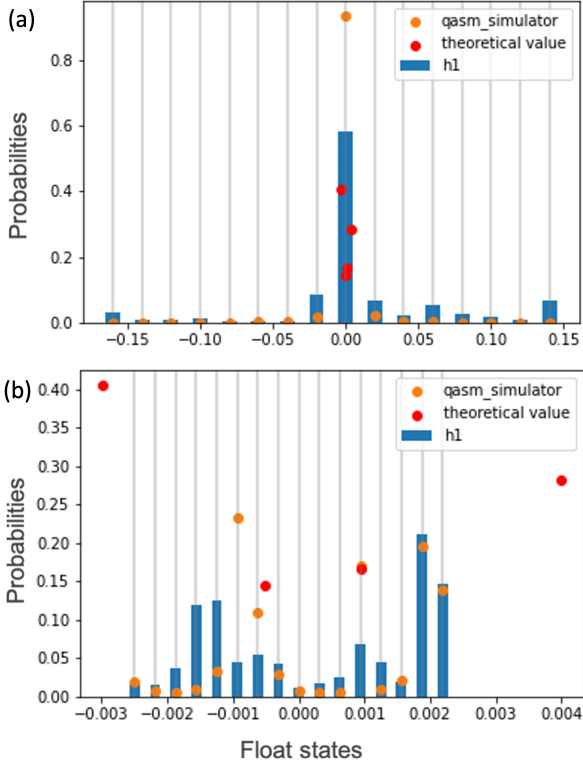


Fig. 4. Probability distributions over the four-bit eigenvalue estimates from the QCL-QPE executions using $e^{iA2\pi\Gamma}$ for $\Gamma = 50 \cdot 2^{-4}$ (a) and $\Gamma = 200$ (b). The blue bars represent the experimental results on the H1-2 machine - 2000 shots (a) and 2000 shots (b). The theoretical (classically calculated) eigenvalues are represented with the red dots and the results from the Qiskit QASM simulator are represented with the orange dots. On (b) as the theoretical eigenvalues exceed the values we can encode, the distribution we observed shows that values overflowed.

proposal is to use the following technique to select the states that best represent the relevant eigenvalues (i.e., Λ_b).

Given the definition of Λ_b (refer to Section IV), we are looking for each eigenvalue, λ_i , that satisfies $|\beta_i/\lambda_i| > \epsilon$. In this particular case, given the four-bit precision, with one bit encoding the sign, the factor $1/\lambda_i$ will be at most 2^3 , and hence it is not significant enough to consider using the mentioned technique. However, a noise-threshold can be used to remove states with close-to-zero probability in the distribution displayed in Figure 5 (b). We then picked states whose probabilities are significantly higher than this threshold. It is straightforward to see in the distribution that the four states indicated with black arrows have probabilities that are higher than the noise-threshold.

We can see that the two largest eigenvalues, computed classically and indicated with the red dots and the green arrows in Figure 5 (b) are in the middle of two vertical lines, which represent possible eigenvalue estimates. As a consequence, we can state that the probabilities corresponding to each of these eigenvalues are split into their neighboring states. As such, we

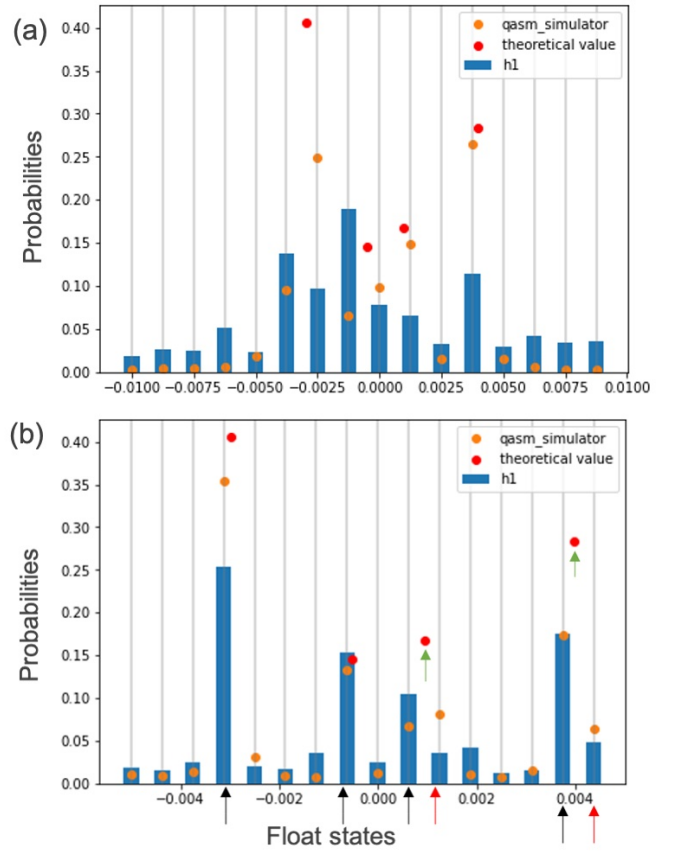


Fig. 5. Probability distributions over the four-bit eigenvalue estimates from the QCL-QPE run using $e^{iA2\pi\gamma}$ for $\gamma = 50$ (a) and $\gamma = 100$. The blue bars represent the experimental results on the H1-2 machine - 2000 shots (a), 1000 shots (b). The theoretical (classically calculated) eigenvalues are represented with the red dots and the results from the Qiskit QASM simulator are represented with the orange dots.

can also consider the states with higher probability indicated with the red arrows as estimates of the elements in Λ_b .

Note that we have detected this probability splitting in neighboring states by looking at the classically calculated eigenvalues. As the eigenvalues might have an infinite binary decomposition, thus we expect this probability splitting to exist regardless of the precision. Therefore, we also used the Qiskit QASM quantum simulator. The probabilities of the neighboring states calculated on simulator (indicated with the red arrows) are significantly higher than the noise-threshold for the simulation results. This allows us to consider these states as estimates of the elements in Λ_b . In addition, more complex resolution methods, such as multiple scaling factors, might be used in future work.

We have built two possible sets of four-bit estimates to represent the elements in Λ_b . These are: the four estimates indicated with the black arrows and the six estimates indicated with both the black and the red arrows. In Section IV-B and IV-C we will compare the performance of the proposed implementation of HHL circuits using these two sets to control the rotations.

IV. END-TO-END DEMONSTRATION OF PORTFOLIO OPTIMIZATION

In this section we introduce the formulation of the portfolio-optimization problem as a QLSP, which makes it compatible to be solved with HHL. In addition to portfolio optimization, quantum algorithms have been designed that are applicable to various other financial applications [27, 28]. We show both simulation and experimental results on hardware for solving this problem using the proposed approach of Hybrid HHL enhanced with Dynamic Quantum Circuits on the Quantum System Model H1-2.

A. Portfolio Optimization as a QLSP

HHL has been proposed as a possible solver for a specific portfolio-management problem [29], known as mean-variance portfolio optimization. Given a set of \tilde{N} assets, this problem requires the following quantities as inputs: the *historical covariance matrix* $\Sigma \in \mathbb{R}^{\tilde{N} \times \tilde{N}}$, the *expected returns* $\vec{r} \in \mathbb{R}^{\tilde{N}}$, and the *prices* $\vec{p} \in \mathbb{R}^{\tilde{N}}$ of the assets. Its objective is to minimize the *risk*, represented by the quadratic form $\vec{w}^T \Sigma \vec{w}$, subject to the desired *expected total return* $\mu \in \mathbb{R}$ and *budget* $\xi \in \mathbb{R}$. The solution $\vec{w} \in \mathbb{R}^{\tilde{N}}$ is the *allocation vector* that weighs each asset in the portfolio.²

This problem can be stated as a convex quadratic program:

$$\underset{\vec{w} \in \mathbb{R}^{\tilde{N}}}{\text{minimize}} \quad \vec{w}^T \Sigma \vec{w} \quad : \quad \xi = \vec{p}^T \vec{w}, \quad \mu = \vec{r}^T \vec{w}$$

This quadratic program can be reformulated as a linear system by using the method of Lagrange multipliers, resulting in the following equation:

$$\begin{bmatrix} 0 & 0 & \vec{r}^T \\ 0 & 0 & \vec{p}^T \\ \vec{r} & \vec{p} & \Sigma \end{bmatrix} \begin{bmatrix} \eta \\ \theta \\ \vec{w} \end{bmatrix} = \begin{bmatrix} \mu \\ \xi \\ \vec{0} \end{bmatrix} \quad (2)$$

where $\eta, \theta \in \mathbb{R}$ are the Lagrange multipliers. We will denote this linear system by $A\vec{x} = \vec{b}$, with $A \in \mathbb{R}^{N \times N}$ and $\vec{x}, \vec{b} \in \mathbb{R}^N$, where $N = \tilde{N} + 2$. A quantum state representing the solution, up to a normalization constant, can be obtained by solving the corresponding QLSP using HHL. This can be done because the covariance matrix, Σ , is Hermitian, and so A is Hermitian too. The resulting quantum state $|x\rangle = |\eta, \theta, w\rangle$ allows us to recover $|w\rangle$.

Following this approach, Rebentrost and Lloyd [29] have shown how to use the quantum state produced by HHL to make calculations that are of interest to the financial industry. For instance, given the optimal portfolio state, one can measure the portfolio's risk, or compare, through a controlled-SWAP test [30], the optimal portfolio to another candidate portfolio (e.g., one offered by a third party) that has been loaded onto a quantum state. The result of this comparison can then be used to decide which portfolio to invest in.

²Since the solution is a weight vector, the budget is only a scaling parameter and can be set to 1. Moreover, in order to compare portfolio performances, the return of a portfolio is usually expressed as a percentage instead of a monetary amount. With a simple change of variables, the problem can be reformulated in these terms.

For the hardware demonstrations we considered a portfolio-optimization problem with two S&P 500 assets. After considering the two constraints, the matrix A of the linear system is of size 4×4 . This QLSP corresponds to the one employed in the previous sections to benchmark QCL-QPE and for obtaining the eigenvalue estimates. For the execution on hardware, we followed the same considerations made in Section III-A.

Based on the results of the QCL-QPE benchmark in Section III-A, we run the separate QCL-QPE procedure, Step (a) in Fig. 2, for estimating the eigenvalues to four bits. We use the four-bit estimates to calculate the angles for the rotations in the eigenvalue inversion. Instead of using these four-bit estimates to control the rotations, we map them to three-bit estimates. By doing this, we are reducing the number of qubits required in the HHL circuit while employing a more precise angles for the rotations. Apart from the separate component using QCL-QPE, HHL will use the standard QPE circuit in Step (d) of the algorithm with three ancillas. In subsection IV-B we benchmark the eigenvalue inversion component of HHL implemented by inverting the eigenvalue estimates obtained by QCL-QPE. Then in subsection IV-C we show experimental results for the execution of the end-to-end HHL for solving the portfolio-optimization problem mentioned above on hardware and some other problems in simulation.

B. Performance of the Eigenvalue Inversion

If we run the HHL circuit up to the eigenvalue inversion component, ideally a measurement of the register T will return an n -bit estimate of one of the relevant eigenvalues, and S will return a superposition of the corresponding eigenvectors, as shown in the final state in (1). Unfortunately, this is not necessarily true, mainly due to hardware noise. To quantify this noise as a function of the number of ancillas and determine the size of the eigenvalue register in HHL, we tested this component.

To do so, we ran circuits that perform the transformation represented by (3), with the register T consisting of two, three or four qubits. For these experiments, we used one of the eigenvalues of A , λ , that was estimated to four bits in Section III-B. The estimate was truncated in the cases where T consisted of two or three qubits. We took $C := \min\{|\tilde{\lambda}_i|\}_{i=0}^{m-1}$, and defined the corresponding rotation angle to be $2 \arcsin(C/\lambda)$.

In addition, the register S was initialized with the eigenstate $|u\rangle$ corresponding to λ . The first term of the final state in the mapping in (3) represents the desired output state. Whereas, the second term represents the presence of noise.

$$\begin{aligned} |0\rangle \otimes |\tilde{\lambda}\rangle_T |u\rangle_S &\rightarrow \\ &\left(\sqrt{1 - \frac{C^2}{\lambda^2}} |0\rangle + \frac{C}{\lambda} |1\rangle \right) \otimes |\tilde{\lambda}\rangle_T |u\rangle_S \\ &+ \sum_{j=0}^M (\alpha_j |0\rangle + \beta_j |1\rangle) \otimes |\eta_j\rangle_T |\sigma_j\rangle_S \quad (3) \end{aligned}$$

We ran the circuits on the Quantinuum H1-2 system, and we measured all registers. Figure 6 displays the probability distributions of certain events that occur after measuring all of the registers for each of the three circuits executed. The events “0” (success) and “1” (failure) correspond to the post-measurement states $|0\rangle|\tilde{\lambda}\rangle_T|u\rangle_S$ and $|1\rangle|\tilde{\lambda}\rangle_T|u\rangle_S$ respectively (first term in the final state mapping in (3)). Tracing out the rotation ancilla, the event “other” corresponds to the post-measurement state of registers T and S not being the product state $|\tilde{\lambda}\rangle_T|u\rangle_S$ (second term of the final state in (3)).

We conclude that increasing the number of ancillary qubits, which are the ancillas in the end-to-end HHL, raises the probability of “other”. This represents the probability of measuring noise in both the T and S registers. The noise is represented by states that do not correspond to the estimated eigenvalue and its eigenstate. Moreover, we see that for four ancillas the experimental probabilities and the theoretical values represented by the dotted lines disagree.

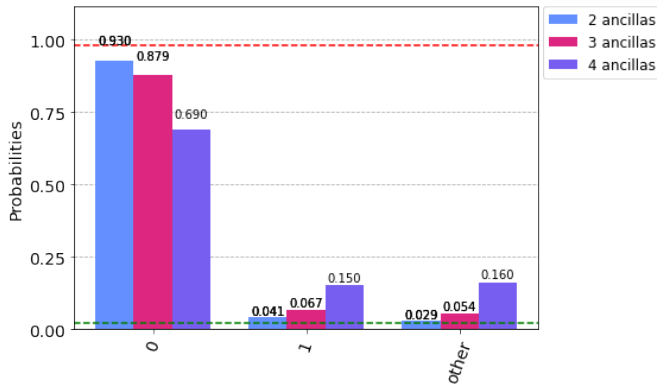


Fig. 6. Probability distributions of previously mentioned events that occur after measuring all of the registers after the eigenvalue inversion on the Quantinuum H1-2 device with 1000 shots. The red dotted line represents the theoretical probability of the failure (“0”) event and the green dotted line that of success (“1”) event.

Even though it seems that the best choice is to use two ancillas, it will not provide enough precision for the QPE to separate the eigenvalues for a proper eigenvalue inversion. Therefore, we decided to employ three ancillas. This result is in agreement with the conclusion reached from the results of the standard QPE benchmarks in Section III-A.

Now that we have determined the number of ancillas for the HHL circuit, we implemented it and we studied the number of controlled rotations and the circuit depth, in terms of ZZMax, of the eigenvalue inversion circuit. In Table III, we show a comparison for the three implementations: the uniformly controlled rotation gate and the proposed eigenvalue inversion circuit that inverts on the estimates of the relevant eigenvalues. For this approach (“Relevant”) there are two implementations: one where the rotations are conditioned on four estimates and another one where the rotations are controlled on six estimated eigenvalues respectively (refer to Section III-B). In all the cases, the circuits consisted of three control ancillary qubits and one rotation ancillary qubit.

| | Uniformly | Relevant | Relevant |
|-----------|-----------|----------|----------|
| Rotations | 7 | 4 | 6 |
| Depth | 138 | 80 | 120 |

TABLE III
COMPARISON OF THE NUMBER OF ROTATIONS AND ZZMAX DEPTH OF THE DIFFERENT EIGENVALUE INVERSION CIRCUITS.

The number of rotations in each approach was determined as follows. According to the classical post-processing, we implemented two circuits conditioning the rotations on two sets of estimates of Λ_b respectively, one with four estimates and another one with six. In this approach, one could rotate on $|0\rangle$ as it can represent an eigenvalue that got rounded to 0 when reducing the bit precision from n to r bits. For example, in Figure 5 (b) the first black arrow to the right of the x -axis origin, corresponds to the $|000\rangle$ state when represented with three bits. The rotation angle is determined based on the four-bit representation $|1111\rangle$, i.e., -1 in two’s complement representation. In contrast, the uniformly controlled rotation approach excludes the zero state, for the reasons explained in Section IV. As a consequence, in this approach the rotations employing three control ancillas are conditioned on seven eigenvalue estimates.

We see in Table III that our proposed eigenvalue inversion circuits are significantly shallower: a reduction of 42% and 13% in depth when conditioning on four and six estimates respectively. What is more, the angles for the controlled rotations $\{\theta_i\}_{i=0}^{m-1}$ are estimated from eigenvalue estimates of Λ_b , which utilized more precision in our approach. Therefore, for these two reasons, we expect to obtain a more accurate estimation of the solution to the linear system by executing our proposed classical-quantum hybrid HHL with quantum conditional logic on NISQ devices.

In the next subsection we will show the results from executing end-to-end hybrid HHL with dynamic quantum circuits for solving portfolio-optimization problems. A way of comparing the estimation of the best portfolio to the classical calculated solution is by using a controlled-SWAP test [30] between the quantum states that represent them. In the next section we show the results obtained with our proposed implementation of HHL and the implementation using the uniformly controlled rotations.

C. SWAP Test Between the Portfolio State and Classical Solution

The controlled-SWAP test can be used to compute the magnitude of the inner product between the quantum state that represents the allocation vector produced by HHL and the classical solution loaded onto a quantum state [31].

We added a new qubit to the HHL circuit called the *swap ancillary qubit*, and we loaded the normalized classically calculated solution to the linear system, i.e., \vec{x}_c , onto this qubit. Then we ran HHL and the controlled-SWAP test between the HHL output state $|x\rangle$ and the quantum state encoding the classical solution $|x_c\rangle$.

We executed the circuits in the Qiskit statevector simulator and on the Quantinuum H1-2 hardware for the three different approaches discussed before: the uniformly controlled rotation gate and the proposed eigenvalue inversion circuit that inverts on the estimates of the relevant eigenvalues, conditioning on four and six estimates respectively. These are the sets introduced in Section III-B.

We measured the rotation and swap ancillary qubits. With the results from the measurements of these two qubits using 3000 shots, we calculated the inner product between the quantum states as:

$\sqrt{2 \frac{P(|10\rangle)}{P(|10\rangle)+P(|11\rangle)}} - 1$, where P represents the probability of measuring the respective quantum state. The most-significant qubit corresponds to the rotation ancilla, where a post-measurement state of $|1\rangle$ corresponds to success. A uniform distribution would result in a inner product equal to 0.

We show the inner products as well as the circuit depths and the number of controlled rotations for the three approaches, in Table IV. Regarding the simulation results, the proposed eigenvalue inversion rotations conditioned on six eigenvalues increased the magnitude of the inner product by 40.7% over the original method with a uniformly controlled rotation. This is due to the four-bit estimation used in our method for computing the rotation angles, compared to the three-bit precision in the previously mentioned method.

| | Uniform | Proposed | Proposed |
|------------|---------|----------|----------|
| Rotations | 7 | 4 | 6 |
| Depth | 272 | 214 | 254 |
| Simulation | 0.59 | 0.49 | 0.83 |
| H1-2 | 0.42 | - | 0.46 |

TABLE IV

COMPARISON OF THE NUMBER OF ROTATIONS AND CIRCUIT DEPTH OF THE EIGENVALUE INVERSION COMPONENTS OF BOTH THE PROPOSED HHL (“PROPOSED”) AND HHL USING THE UNIFORMLY CONTROLLED ROTATION GATE (“UNIFORM”). WE ALSO COMPARE THE MAGNITUDE OF THE INNER PRODUCTS CALCULATED WITH THE QISKIT STATEVECTOR SIMULATOR AND THE QUANTINUUM SYSTEM MODEL H1-2 WITH 3000 SHOTS. THE CIRCUIT DEPTH IS CALCULATED IN TERMS OF THE ZZMAX GATES.

We achieved a smaller inner product with the proposed HHL when conditioning the rotations on four eigenvalue estimates, instead of six, on simulator. The reason for this is that the set of four eigenvalue estimates is an incomplete representation of the elements of Λ_b due to an inefficient classical post-processing over the probability distribution of the eigenvalue estimates displayed in Figure 5 (b). As discussed, not all of the classically calculated values coincide with the experimental results. In order to reach a better inner product, we had to detect that, in some cases, the probability mass was split between the closest approximations to the eigenvalues. This was possible by analyzing the results of the Qiskit QASM simulator together with experimental results. This shows the importance of an efficient classical post-processing that allows for determining the controls and angles for the rotations in the eigenvalue inversion step.

We can see from the results of the experiments on the Quantinuum System Model H1-2 that the calculated inner products are significantly smaller than the ones calculated using the Qiskit statevector simulator. This stems from the fact that the circuits executed are very deep for NISQ devices. Nevertheless, the proposed HHL, controlling on the six estimates, performed better than the uniformly controlled rotation version. This is because our novel approach employs more precision in bits for the rotation angles, and the shallower circuits used are less prone to hardware noise.

The proposed classical-quantum hybrid HHL with dynamic quantum circuits can be easily applied to any QLSP, including portfolio-optimization problems for portfolios of any given size. Particularly, we show how the algorithm works for more assets. We considered two portfolio-optimization problems consisting of 6 and 14 S&P 500 assets respectively. We ran our proposed approach of HHL for these two problems followed by the controlled-SWAP test on the Qiskit statevector simulator. The results from the controlled-SWAP test were used to calculate the inner product between the quantum state produced by HHL and the optimal quantum state computed classically.

We ran Step (a) and (b) in Figure 2, for both problems. The rotations in the eigenvalue inversion circuits were condition on these estimates respectively: four estimates for the 6 assets problem and five for the 14 assets problem. In both cases we used six ancillary qubits.

Even though we are running fewer controlled rotations in the proposed approach, the number of qubits required is still significant: 14 for 6 assets and 16 for 14 assets. The circuits are also still very deep. These characteristics prevent us from running these experiments on real hardware. Nevertheless, we can calculate the inner products using the Qiskit statevector simulator. We compare the number of controlled rotations, the circuit depths and the inner products, in Table V.

We can see that for both sets of assets, the inner products calculated with the proposed implementation of HHL (“Prop HHL”) are significantly high (very close to one). The inner products obtained for the 14 assets problem are slightly higher than for the 6 assets one. A reason for this is that the eigenvalue inversion implementation depends on the classical post-processing of the probability distribution obtained with the separate QCL-QPE routine. And in some cases, this processing may estimate the elements of Λ_b more accurately than in others. A future research project could be improving the post-processing technique to better identify the elements of Λ_b .

Moreover, the number of rotations, and as a result the circuit depths, are an order of magnitude less in the proposed implementation in comparison to the uniformly controlled rotation circuit. These results support the evidence that, on a sufficiently powerful quantum computer containing enough qubits and capable of handling the required circuit depths, the proposed implementation of HHL will produce accurate results when optimizing portfolios with many assets.

| | Prop HHL | HHL | Prop HHL | HHL |
|--------|----------|-------|----------|-------|
| Assets | 6 | 6 | 14 | 14 |
| Rots | 4 | 64 | 5 | 64 |
| Depth | 1877 | 12911 | 6514 | 11786 |
| Prod | 0.86 | 0.92 | 0.98 | 0.95 |

TABLE V

COMPARISON OF THE PROPOSED HHL (“PROP HHL”) AND HHL IMPLEMENTED WITH UNIFORMLY CONTROLLED ROTATION GATE FOR THE PROBLEMS WITH 6 AND 14 ASSETS. BOTH ALGORITHMS ARE AUGMENTED WITH CONTROLLED-SWAP TEST CIRCUITS. THE COMPARISON INCLUDES THE INNER PRODUCTS (“PROD”) CALCULATED BY USING MEASUREMENTS COLLECTED FROM THE QISKIT STATEVECTOR SIMULATOR AND THE NUMBER OF ROTATIONS IN THE EIGENVALUE INVERSION COMPONENT (“ROTS”). THE CIRCUIT DEPTH IS CALCULATED IN TERMS OF THE ZZMAX GATES.

V. DISCUSSION ON APPROACHES FOR EIGENVALUE INVERSION

As mentioned, different approaches have been proposed for implementing the eigenvalue inversion rotations in HHL. The main differences between them is their complexity and ancilla requirement.

We compare four methods to invert eigenvalues encoded on r -qubits. Quantum arithmetic [16] first approximates the arcsine function and then it rotates the eigenvalues with r Ry gates. The three other techniques directly inverts the eigenvalues by decomposing multi-control rotation gates in different fashion, either with ancilla, as it is the case with Gray code [17] and Control Rotation [10], or with extra ancillas, as it is with V-Chain [10]. The last two methods provides a reduced complexity when inverting only m eigenvalues, instead of the 2^r possible ones.

The Uniformly Controlled Rotation gate mentioned across the article was implemented using Control Rotation with $m = 2^r$ and we compared it to Control Rotation with a smaller number m , the estimated relevant eigenvalues.

| Inverter Name | CNOT Count | Ancilla Count |
|------------------|----------------------|---------------|
| V-Chain | $12m(r-1)$ | $r-1$ |
| Gray code | 2^r | 0 |
| Control Rotation | $m(96r-380)^\dagger$ | 0 |

TABLE VI

COMPARISON OF CNOT AND ANCILLAS COUNT FOR DIFFERENT IMPLEMENTATIONS OF THE EIGENVALUE INVERSION COMPONENT OF HHL

If using ancillas, one can use the V-Chain method or quantum arithmetic, the later is only considered by its authors in the case of using at least few hundreds of qubits. For this reason, we leave this approach aside from the comparison of CNOT and ancilla counts in Table VI. For a small number of qubits, one would resort to the V-Chain implementation.

In the scenario in which we do not use ancillas, if $r < 9$, one should use the Gray code, independently of the value of m . For bigger values of r , one could prefer the control rotation methods even if $m = O(2^r)$.

[†]valid for $r \geq 6$. For $r < 6$, CNOT count is larger than 2^r

This paper leveraged control rotation methods to invert eigenvalues, even if sub-optimal on today’s hardware, it shows a path for the future hardware and the techniques developed like the eigenvalue selection and post-processing can enhance Gray code or V-Chain implementations.

VI. CONCLUSIONS

In this work, we improved on the Hybrid HHL introduced by Lee *et al.* with dynamics quantum circuits (DQCs) [11], which enables the insertion of mid-circuit measurements, resets, and quantum conditional logic (QCL). By leveraging these newly-available hardware features we implemented the QPE variant, the QCL-QPE, for estimating the relevant eigenvalues a part of the Hybrid HHL. This QCL-QPE version of QPE is particularly suitable for NISQ devices since it addresses the scarcity of qubits by using just one ancilla for an arbitrary bit precision. It also tackles the fact that faulty two-qubit gates are currently the dominant source of error by replacing two-qubit gates with one-qubit gates controlled by classical bits.

We experimentally showed that QCL-QPE achieves high fidelity, between experimental and simulated measurement distributions, for three-bit precision. Particularly, for four-bit estimations, QCL-QPE achieved a higher fidelity than the standard QPE.

Our contributions are also algorithmic, we developed an algorithm that optimizes the scaling parameter γ for the Hamiltonian simulation required by QCL-QPE. We showed that the scaling of A by the γ , obtained with the algorithm, enabled resolving the relevant eigenvalues in the output distribution of QCL-QPE more accurately. These n -bit estimates of the relevant eigenvalues are used to calculate the angles for the rotations in the eigenvalue inversion component. Then, they are mapped to a small number of bits, r , so as to control the rotations on these estimates and reduce the number of qubits required. In comparison to the uniformly controlled rotation approach, the number of rotations in this implementation is smaller, and as a consequence, the circuit is significantly shallower and the number of qubits required is reduced.

The main aim of this work is to allow for hardware demonstrations of quantum algorithms for tackling a practical use case in near-term hardware. We do not claim any speedup with our method, it is a step forward implementation on real hardware. We do a comparative analysis of different approaches for the eigenvalue inversion component of HHL in terms of CNOT and ancilla count and we identify different regimes where we see advantage of some methods over others.

We executed separate components of the Hybrid HHL enhanced with dynamic quantum circuits and end-to-end implementation on real hardware, the trapped-ion Quantum System Model H1-2, to optimize a S&P 500 portfolio by casting this problem as a QLSP. To the best of our knowledge, this is the largest-to-date execution of HHL with a two-qubit gate depth up to 254. We obtained, with great fidelity, the optimal allocation vector represented as a quantum state.

We also showed that the proposed eigenvalue inversion circuit is significantly more efficient than the uniformly con-

trolled rotation gate method. This is because we reduced the number of controlled rotations, and as a consequence, the circuit depth and the number of qubits. What is more, this approach is more suitable for NISQ devices, in comparison to Lee *et al.* work, since QCL-QPE requires less qubits and coherence time.

Moreover, we solved a practical use case on quantum hardware. We calculated the inner product between the quantum portfolio state obtained with the end-to-end execution of our approach for the Hybrid HHL and the classically calculated solution loaded as a quantum state. Using the proposed approach, we obtained a higher inner product than the uniformly controlled rotations method when executing on hardware and in the Qiskit statevector simulator.

ACKNOWLEDGMENTS

We thank Tony Uttley, Brian Neyenhuis and the rest of the Quantinuum Quantum Solutions team for assisting us on the execution of the experiments on the Quantinuum System Model H1-2. We also thank Michele Mosca and his team at University of Waterloo for their insights, and Aram Harrow from Massachusetts Institute of Technology for his precious feedback.

DISCLAIMER

This paper was prepared for information purposes by the Global Technology Applied Research group of JPMorgan Chase Bank, N.A.. This paper is not a product of the Research Department of JPMorgan Chase Bank, N.A. or its affiliates. Neither JPMorgan Chase Bank, N.A. nor any of its affiliates make any explicit or implied representation or warranty and none of them accept any liability in connection with this paper, including, but limited to, the completeness, accuracy, reliability of information contained herein and the potential legal, compliance, tax or accounting effects thereof. This document is not intended as investment research or investment advice, or a recommendation, offer or solicitation for the purchase or sale of any security, financial instrument, financial product or service, or to be used in any way for evaluating the merits of participating in any transaction.

REFERENCES

[1] A. W. Harrow *et al.*, “Quantum algorithm for linear systems of equations,” *Physical review letters*, vol. 103, no. 15, p. 150502, Oct. 2009, doi: 10.1103/PhysRevLett.103.150502.

[2] S. Aaronson, “Read the fine print,” *Nature Physics*, vol. 11, no. 4, pp. 291–293, Apr. 2015, doi: 10.1038/nphys3272.

[3] J. Preskill, “Quantum computing in the nisq era and beyond,” *Quantum*, vol. 2, p. 79, Aug. 2018, doi: 10.22331/q-2018-08-06-79.

[4] C. Bravo-Prieto *et al.*, “Variational quantum linear solver,” arXiv:1909.05820.

[5] H.-Y. Huang *et al.*, “Near-term quantum algorithms for linear systems of equations,” 2019, arXiv:1909.07344.

[6] Y. Lee *et al.*, “Hybrid quantum linear equation algorithm and its experimental test on ibm quantum experience,” *Scientific reports*, vol. 9, no. 1, pp. 1–12, Mar. 2019, doi: 10.1038/s41598-019-41324-9.

[7] M. Zhang *et al.*, “Improved circuit implementation of the hhl algorithm and its simulations on qiskit,” *Scientific Reports*, vol. 12, no. 1, p. 13287, 2022.

[8] L. Ruiz-Perez *et al.*, “Quantum arithmetic with the quantum fourier transform,” *Quantum Information Processing*, 16(6):152, 2017, vol. 16, no. 6, p. 125, Apr. 2017, doi: 10.1007/s11128-017-1603-1.

[9] M. Möttönen *et al.*, “Transformation of quantum states using uniformly controlled rotations,” *Quantum Information and Computation*, vol. 5, no. 6, pp. 467–473, Sep. 2019, doi: 10.26421/QIC5.6-5.

[10] A. Barenco *et al.*, “Elementary gates for quantum computation,” *Physical Review A*, vol. 52, no. 5, pp. 3457–3467, Nov. 1995. DOI: 10.1103/physreva.52.3457. [Online]. Available: <https://doi.org/10.1103/physreva.52.3457>.

[11] A. Córcoles *et al.*, “Exploiting dynamic quantum circuits in a quantum algorithm with superconducting qubits,” *Physical Review Letters*, vol. 127, no. 10, Aug. 2021. DOI: 10.1103/physrevlett.127.100501. [Online]. Available: <https://doi.org/10.1103%2Fphysrevlett.127.100501>.

[12] R. B. Griffiths *et al.*, “Semiclassical fourier transform for quantum computation,” *Physical Review Letters*, vol. 76, no. 17, pp. 3228–3231, Apr 1996, doi: 10.1103/PhysRevLett.76.3228.

[13] S. Beauregard, “Circuit for shor’s algorithm using $2n+3$ qubits,” *Quantum Information and Computation*, vol. 3, no. 2, pp. 175–185, Mar. 2003, doi: 10.26421/QIC3.2-8.

[14] M. Mosca *et al.*, “The hidden subgroup problem and eigenvalue estimation on a quantum computer,” in *NASA International Conference on Quantum Computing and Quantum Communications*, doi: 10.1007/3-540-49208-9_15, Springer, Feb. 1998, pp. 174–188.

[15] X. Zhang *et al.*, “Simplified experimental scheme of quantum algorithm for solving linear equations with single photons,” *Optics Express*, vol. 27, no. 3, pp. 3369–3378, 2019.

[16] T. Häner *et al.*, “Optimizing quantum circuits for arithmetic,” arXiv:1805.12445, 2018.

[17] M. Möttönen *et al.*, “Quantum circuits for general multiqubit gates,” *Physical review letters*, vol. 93, no. 13, p. 130502, Sep. 2004, doi: 10.1103/PhysRevLett.93.130502.

[18] H. Mohammadbagherpoor *et al.*, “Experimental challenges of implementing quantum phase estimation algorithms on ibm quantum computer,” arXiv:1903.07605, 2019.

[19] M. Dobšiček *et al.*, “Arbitrary accuracy iterative quantum phase estimation algorithm using a single ancillary qubit: A two-qubit benchmark,” *Physical Review A*,

vol. 76, no. 3, p. 030 306, Sep. 2007, doi: 10.1103/PhysRevA.76.030306.

- [20] J. Pino *et al.*, “Demonstration of the trapped-ion quantum ccd computer architecture,” *Nature*, vol. 592, no. 7853, pp. 209–213, Apr. 2021, doi: 10.1038/s41586-021-03318-4.
- [21] *Quantinuum system model H1 product data sheet [retrieved 08/30/2022]*. URL: \NoCaseChange{<https://www.quantinuum.com/products/h1>}.
- [22] G. Aleksandrowicz *et al.*, “Qiskit: An open-source framework for quantum computing,” *zenodo*, 2019, doi: 10.5281/zenodo.2562111.
- [23] S. Sivarajah *et al.*, “[ket): A retargetable compiler for nisq devices,” *Quantum Science and Technology*, vol. 6, no. 1, p. 014 003, Nov. 2020, doi: 10.1088/2058-9565/ab8e92.
- [24] A. Gilyén *et al.*, “Quantum singular value transformation and beyond: Exponential improvements for quantum matrix arithmetics,” in *Proceedings of the 51st Annual ACM SIGACT Symposium on Theory of Computing*, doi: 10.1145/3313276.3316366, Jun. 2019, pp. 193–204.
- [25] M. A. Nielsen *et al.*, *Quantum Computation and Quantum Information*. Cambridge University Press, 2000.
- [26] I. Kerenidis *et al.*, “Quantum gradient descent for linear systems and least squares,” *Physical Review A*, vol. 101, no. 2, Feb. 2020, doi: 10.1103/physreva.101.022316, ISSN: 2469-9934.
- [27] D. Herman *et al.*, “Quantum computing for finance,” *Nature Reviews Physics*, pp. 1–16, 2023.
- [28] M. Pistoia *et al.*, “Quantum machine learning for finance iccad special session paper,” in *2021 IEEE/ACM International Conference On Computer Aided Design (ICCAD)*, IEEE, 2021, pp. 1–9.
- [29] P. Rebentrost *et al.*, “Quantum computational finance: Quantum algorithm for portfolio optimization,” 2018, arXiv:1811.03975.
- [30] *Tests of quantum information (US Patent 7,559,101 B2)*, Beausoleil, R. G. et al., 2008.
- [31] H. Buhrman *et al.*, “Quantum fingerprinting,” *Physical Review Letters*, vol. 87, no. 16, p. 167 902, Sep. 2001, doi: 10.1103/PhysRevLett.87.167902.